FULL-LENGTH PAPER

Structure, dynamics, and stability of the globular domain of human linker histone H1.0 and the role of positive charges

Jacob H. Martinsen[1] | Daniel Saar[1] | Catarina B. Fernandes[1] |
Benjamin Schuler[2,3] | Katrine Bugge[1] | Birthe B. Kragelund[1]

[1]REPIN and the Structural Biology and NMR Laboratory, The Linderstrøm-Lang Centre for Protein Science, Department of Biology, University of Copenhagen, Copenhagen, Denmark

[2]Department of Biochemistry, University of Zurich, Zurich, Switzerland

[3]Department of Physics, University of Zurich, Zurich, Switzerland

Correspondence
Katrine Bugge and Birthe B. Kragelund, REPIN and the Structural Biology and NMR Laboratory, The Linderstrøm-Lang Centre for Protein Science, Department of Biology, University of Copenhagen, Ole Maaloes Vej 5, DK-2200 Copenhagen N, Denmark.
Email: katrine.bugge@bio.ku.dk and bbk@bio.ku.dk

Funding information
Novo Nordisk Foundation Challenge program, Grant/Award Number: NNF18OC0033926; Novo Nordisk Foundation Synergy program, Grant/Award Number: NNF15OC0016670; Novo Nordisk Foundation, Grant/Award Number: NNF18OC0032996

Abstract

Linker histone H1 (H1) is an abundant chromatin-binding protein that acts as an epigenetic regulator binding to nucleosomes and altering chromatin structures and dynamics. Nonetheless, the mechanistic details of its function remain poorly understood. Recent work suggest that the number and position of charged side chains on the globular domain (GD) of H1 influence chromatin structure and hence gene repression. Here, we solved the solution structure of the unbound GD of human H1.0, revealing that the structure is almost completely unperturbed by complex formation, except for a loop connecting two antiparallel β-strands. We further quantified the role of the many positive charges of the GD for its structure and conformational stability through the analysis of 11 charge variants. We find that modulating the number of charges has little effect on the structure, but the stability is affected, resulting in a difference in melting temperature of 26 K between GD of net charge +5 versus +13. This result suggests that the large number of positive charges on H1-GDs have evolved for function rather than structure and high stability. The stabilization of the GD upon binding to DNA can thus be expected to have a pronounced electrostatic component, a contribution that is amenable to modulation by posttranslational modifications, especially acetylation and phosphorylation.

KEYWORDS

CD, histone, NMR, nucleosome, protein electrostatics, protein stability, protein structure

1 | INTRODUCTION

Chromatin is the higher-order structure responsible for protecting and condensing the eukaryotic genome in the nucleus. It is composed of repeating units called chromatosomes, made up of nucleosome cores, DNA and linker histone H1 (H1) (or H5 in birds) (Figure 1a). The nucleosome core particle consists of ~147 bp of DNA winding in a left-handed manner around an assembly of eight core histone proteins (two copies of H2A, H2B, H3, and H4 each).[2] The resulting ~200 kDa disk-shaped assembly has a twofold symmetry axis referred to as the
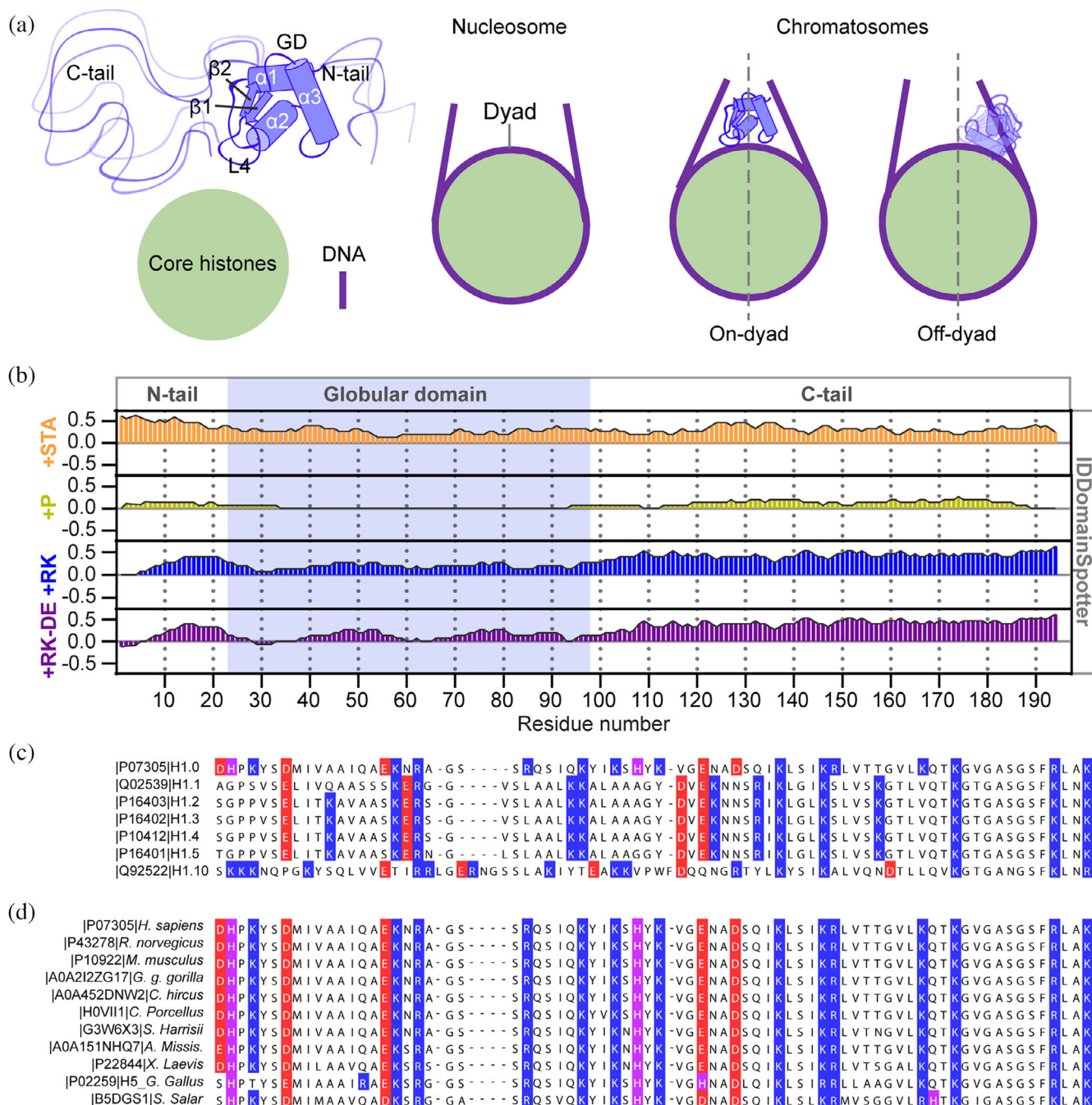
FIGURE 1 Binding modes and primary structures of H1-GDs. (a) Sketches of bound H1-GD (blue), the core histone oligomer (green) and DNA (purple), and their assembly to form a nucleosome or a chromatosome. The GD is folded into the classical "winged" helix-turn-helix DNA binding motif with two antiparallel β-strands, β1 and β2, in the C-terminus, connected by a loop (the β-hairpin). The dyad axis is oriented along the center of the nucleosome and through the central basepair of the DNA. The on-dyad and off-dyad binding modes of the GD are sketched on the right. (b) IDDomainSpotter[1] profiles of human linker histone H1.0. Profiles display scores for +(Ser, Thr, Ala) (orange), +(Pro) (yellow), +(Arg, Lys) (blue), +(Arg, Lys)-(Asp, Glu) calculated over a 15-residue window. (c) Sequences of the seven somatic isoforms of human H1-GD. The predicted pIs of the various isoforms are between 10.2 and 10.3 (not shown). (d) Sequences of H1-GD (H5 from *G. gallus*) from different species. "*A. Missis.*" is abbreviation for "*Aligator mississippiensis*." Asp and Glu are highlighted with red shading, Lys and Arg with blue shading, and His with purple shading

nucleosome dyad passing through the central DNA base pair[3–5] (Figure 1a). H1 compacts the nucleosomes by associating with the two linker DNA segments, as well as

by binding to the DNA that crosses the dyad (Figure 1a).[5–7] In doing so, it impacts many cellular functions,[3,8] for example, it acts as a repressor of

transcription and controls gene expression by modulating access to promotor or enhancer sequences.[8–10]

Several tissue-specific isoforms of H1 exist. In mammals, seven somatic isoforms (designated H1.0–H1.5 and H1.10 [or H1x]), three male germ-line-specific isoforms (H1.6, H1.7, and H1.9) and an oocyte-specific isoform (H1.8) have been identified.[11] H1.0 can be considered the major isoform, being expressed independently of the cell cycle and accumulating in terminally differentiated cells, where it has been suggested to replace somatic isoforms.[12] H1.0 is a highly basic protein, which in humans has a net charge of +53. It is composed of 29% Lys, while Ala and Ser combined account for 25% of the residues, highlighting a low-complexity composition (Figure 1b). It has a tripartite structure consisting of a small, folded domain (called the globular domain [GD]) embedded in a disordered chain making up an N- and C-tail. Human H1.0 consists of 194 residues, of which the disordered N-tail takes up ~23 residues, the disordered C-tail ~97 residues, and the GD ~74 residues. The high positive net charge is distributed throughout the primary structure but with higher density in the C-tail (Figure 1b). All H1 isoforms are highly basic, but the tripartite structure is only conserved in the somatic isoforms, with the GD lacking in the germ-line isoforms. The primary structure of the GD is highly conserved in isoforms H1.1–1.5, whereas it differs slightly in H1.0 and H1.10, in particular for residues with charged side chains (Figure 1c). This is especially noteworthy when considering that the primary structure of the GD is highly conserved across species (Figure 1d), while the primary structure of the N- and C-tails is less conserved among the H1 isoforms, as well as across species.

Knowledge about the roles of H1 in regulating the structure and function of chromatin is limited compared to the core histones.[3,13] The GD is considered the region of H1 primarily responsible for binding to DNA on the nucleosome and has two suggested main binding modes,[14] referred to as "on-dyad" and "off-dyad" binding (Figure 1a). The role of the disordered C-tail has been more challenging to pinpoint; however, the C-tail has been known to increase the affinity for, and residence time on, DNA,[7,15–17] and it affects the assembly of higher-order chromatin structures and controls the openness of the linker DNA.[3,18,19] According to a recent model, the C-tail remains fully disordered in H1 bound to the nucleosome and makes extensive interactions with the linker DNA.[19] The biological role and native occurrence of the off-dyad binding mode remain debated. Several X-ray and cryo-EM as well as integrative structures are available of H1.0-GDs from different species in complex with nucleosomes, which have shown both on- and off-dyad binding modes and different GD

orientations.[14,18,20–26] Öztürk et al. have recently suggested that the different structures can be reconciled by considering the chromatosome as a dynamic ensemble of structures rather than a single conformation, but the study also raises the possibility of differences in experimental conditions.[27] However, it is especially noteworthy that all structures solved with full-length H1 only show the on-dyad binding mode, while the off-dyad binding mode has been found only for GDs without their disordered tails.[13] For isolated GD, previous studies have suggested that the cause of the different binding modes on the nucleosome of chicken H5 (replaces H1 in certain cell types), binding on-dyad, and Drosophila H1, binding off-dyad, is the difference in the positions of just five charged side chains between the two GDs.[14] However, the very recent high-resolution cryo-EM structures of chromatosomes containing full-length human H1.0, H1.4 or H1.10 (2.8–3.1 Å), with slightly different GD primary structures (Figure 1c), all revealed on-dyad binding, but with small differences in the orientations of the GD in the chromatosomes.[18] These differences were ascribed to subtle variations in the interactions of the isoforms with DNA resulting from the small differences in the position of charged side chains.[18] This is consistent with studies showing that the small differences between H1 isoforms result in different levels of condensation of the nucleosome in vitro as well as in their affinity for chromatin in vivo.[28,29] As a result, the different H1 isoforms have differential effects on gene expression.[30] Hence, accumulating evidence suggests that the number and position of positively charged side chains affect chromatosome structure, but that the off-dyad binding mode may not be sampled when the disordered tails are present.

In the winged helix-turn-helix structure of the GD (Figure 1a), the main on-dyad interactions occur through the N-terminal residues of α-helix 2 and the loop of the β-hairpin (dyad interface), while α-helix 3 and the loop between α-helices 1 and 2 contact the linker strands.[13,18] Although NMR assignments and secondary structures of the unbound GD of chicken H1 have been published,[31] the only 3D structure available of an unbound GD is that of H5 from chicken erythrocytes. Its NMR structure was determined in 1987, but it is unavailable in the PDB,[32] and it is similar to the crystal structure of H5, which was later determined to 2.5 Å resolution in 1993 (without the disordered tails).[33] Two subunits were found in the asymmetric unit, differing in the structure of the β-hairpin and its orientation with respect to α-helix 3, leading to the definition of an "open" and a "closed" state of the GD. In the open state, the β-hairpin is extended, while in the closed state it bends toward α-helix 3 and forms hydrophobic contacts. In silico studies have found that the closed state is prevalent for the unbound GD in

solution.[34,35] Further, molecular dynamics simulations have suggested that the GD and the bound linker DNA strands are dynamic in the chromatosome.[18,19,27,34–36] This is supported by experimental observations from fluorescent recovery after photobleaching (FRAP) experiments showing shorter residence times of H1 compared to core histones,[15] and the lower local resolutions of H1-GDs compared to core histones in density maps.[18]

Collectively, the recent progress in understanding the structure and dynamics of H1 in chromatosomes suggests that the position of charged side chains on the GD influence chromatin structure and gene repression. Nonetheless, the structure and dynamics of the human H1-GD in its unbound form remain to be elucidated, as well as the effect of the disordered tails on structure and stability. In the present work, we find that the disordered tails do not markedly eaffect structure or stability of the unbound GD of human linker histone H1.0 (hH1.0$_{GD}$). We determine the solution NMR structure of unbound hH1.0$_{GD}$ and find that the β-hairpin is the only part of the GD undergoing substantial changes in backbone conformation upon complex formation with DNA, changing from a flexible, open conformation, to a restricted, closed conformation. Furthermore, we address the role of its high net charge for structure and stability using circular dichroism (CD) and NMR spectroscopy. We find that while modulating the number of charges of hH1.0$_{GD}$ has little effect on the structure, it affects the stability with a difference in melting temperature of 26 K between hH1.0$_{GD}$ of net charge +5 versus +13. The high number of positive charges renders the GD marginally stable in its unbound state. The stabilization of the GD upon binding to DNA is thus expected to have a pronounced electrostatic component, a contribution that is amenable to modulation by posttranslational modifications, especially acetylation and phosphorylation, which can be important for the regulation of chromatin.

2 | RESULTS

2.1 | The hH1.0$_{GD}$ structure and stability are unaffected by the disordered tails

The function and native conformation of protein domains are often effected by their full-chain context,[37–39] and accumulating evidence suggests that the binding mode of the GD in the nucleosome is influenced by its disordered tails. Hence, we initially investigated whether the structure and thermodynamic properties of the unbound GD were affected by removal of the disordered tails. Based on sequence analysis, residues D24–K97 from human H1.0 were previously identified to

comprise hH1.0$_{GD}$ (Figure 2a).[40] To assess whether the structure and thermodynamic properties of the isolated GD were preserved, thermal denaturation of full-length H1.0 and hH1.0$_{GD}$ was monitored by CD spectroscopy (Figure 2b). A small increase in melting temperature (T$_m$) of hH1.0$_{GD}$ from 320.1 ± 0.1 K for H1.0 to 321.8 ± 0.1 K for hH1.0$_{GD}$, with little difference in ΔH(T$_m$) (184 kJ/mol for H1.0 and 187 kJ/mol for hH1.0$_{GD}$), suggested that the stability of hH1.0$_{GD}$ without the disordered tails was not substantially perturbed. This is consistent with the expected high degree of repulsion between the domains caused by their shared high net positive charge. In support of this observation, most hH1.0$_{GD}$ peaks in the ^{1}H,^{15}N-heteronuclear single quantum coherence (HSQC) NMR spectra overlap fully with the corresponding peaks originating from full-length H1.0 (Figure 2c, gray and blue, respectively). Hence, the structure and stability of the unbound GD are largely unaffected by the presence of its disordered tails.

2.2 | Solution structure and dynamics of hH1.0$_{GD}$ reveal an open loop conformation

The structure and dynamics of hH1.0$_{GD}$ in the unbound state were investigated by NMR spectroscopy. The hH1.0$_{GD}$ resonances were assigned at an ionic strength of 165 mM, pH 7.4, 10°C, using standard heteronuclear NMR backbone experiments (Figure 2d). Manual assignments resulted in 97.4% completeness for backbone resonances and 91.4% for side chain proton resonances. The secondary structure was evaluated by analyzing secondary chemical shifts (SCSs) of C^α calculated using published random coil values[41] (Figure 3a), amide temperature coefficients (Figure 3b), amide hydrogen-to-deuterium exchange protection factors (Figure 3c) and backbone relaxation rates (Figure 3d,e). These data suggest the presence of three fully formed α-helices: K27-E39 (α1), S46-Y58 (α2), and G61-T78 (α3). The three α-helices are connected by loop 1 (K40-S45, L1) and loop 2 (K59-V60, L2), showing only marginally increased dynamics on the pico- to nanosecond timescale compared to the folded regions. In the C-terminal region, residues L81–T84 and S92–R94 displayed SCSs indicative of short β-strands or extended structure, connected by loop 4 (L4). L4 consists of seven residues and represents the most dynamic region of the protein on the pico- to nanosecond timescale.

To describe the tertiary structure of the unbound hH1.0$_{GD}$, the solution structure was determined using 985 NMR-derived restraints, including 170 long-range nuclear overhauser effects (NOEs) (Table 1). From the final 200 water-refined structures, the 20 lowest energy
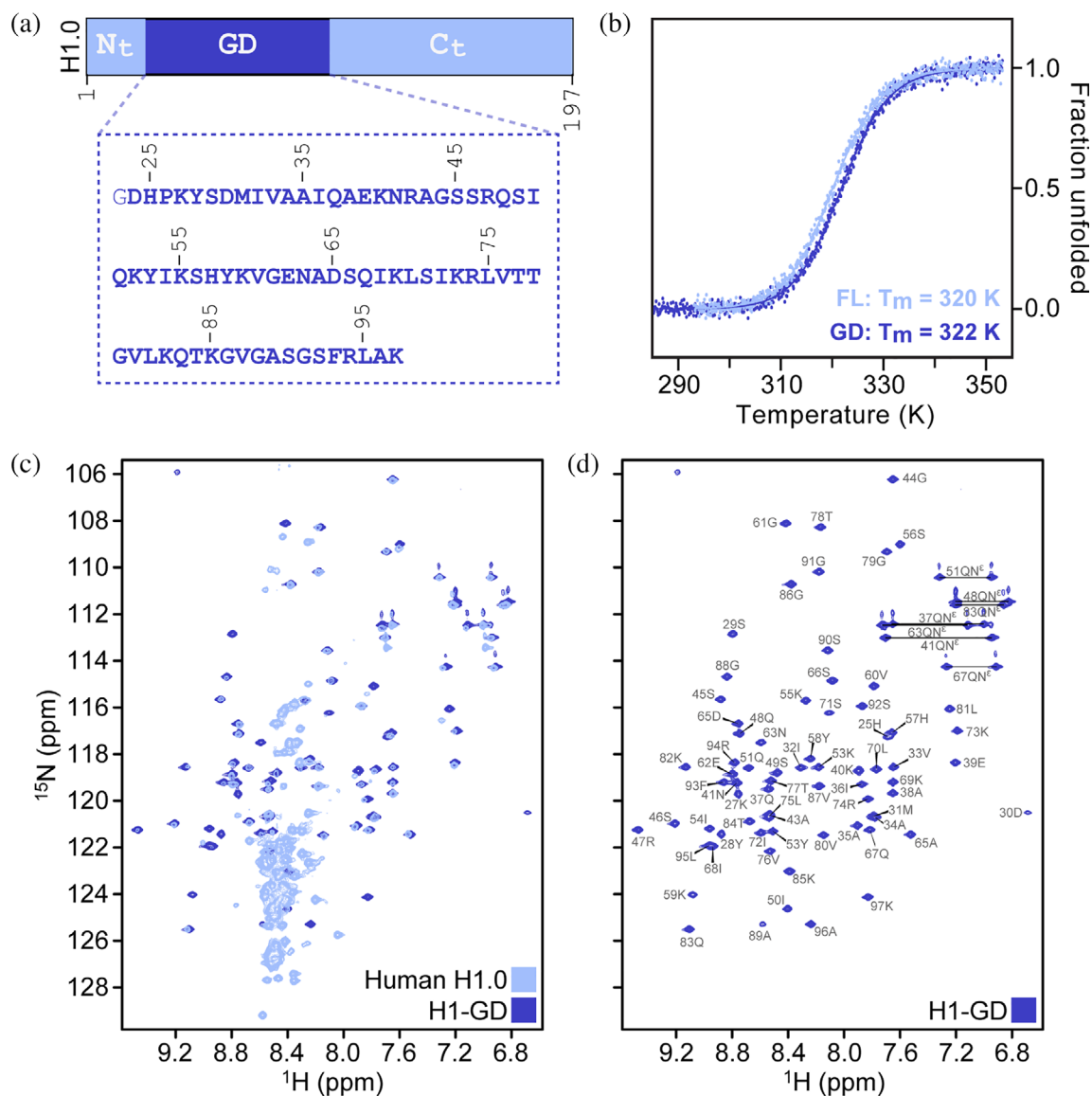
FIGURE 2 Comparison of the structure and stability of human H1.0 and hH1.0$_{GD}$. (a) Domain arrangement of human H1.0, with the primary structure of the hH1.0$_{GD}$ shown below. Note that a Gly remains at the N-terminal from TEV cleavage. (b) Thermal denaturation followed by far-UV CD spectroscopy as changes in $\Theta_{222\,nm}$ as a function of temperature for full H1.0 (light blue) and hH1.0$_{GD}$ (blue). The extracted T$_m$ values are shown as inserts. (c) Overlay of ^{1}H,^{15}N-HSQC spectra of full H1.0 (light blue) and hH1.0$_{GD}$ (blue). (d) Assigned ^{1}H,^{15}N-HSQC spectrum of hH1.0$_{GD}$, acquired at an ionic strength of 165 mM, pH 7.4, 10°C

structures without significant violations (Table 1) were selected to represent the structure of unbound hH1.0$_{GD}$ (Figure 4). As suggested by the backbone relaxation rates, hetNOEs and SCSs, the hH1.0$_{GD}$ mainly consists of the three α-helices α1–α3, which form the classical DNA-binding winged-helix fold (histone fold). In the C-terminal region, residues L81-T84 and S92-R94 form two antiparallel β-strands, β1 and β2, connected by the flexible L4 (Figure 3d,e). This β-hairpin is found to be in the "open" conformation, that is, without contacts to α3, which is supported by the fast backbone dynamics of L4 (Figure 3d,e). The many positively charged side chains of

hH1.0$_{GD}$ are widely distributed on the protein surface (Figures 4b,c and S1).

2.3 | The H1.0$_{GD}$ tertiary structure is conserved across species and complexes

A search in the RCSB PDB depository revealed 10 published structures containing sequences with more than 80% identity to hH1.0$_{GD}$, either H1.0 from *H. sapiens* (PDBs: 6n88, 6n89, 7k5x, 6la8, 6la9, 7dbp), *X. laevis* (PDB: 5nl0) or H5 from *G. gallus* (PDBs: 4qlc, 5wcu, 1hst)
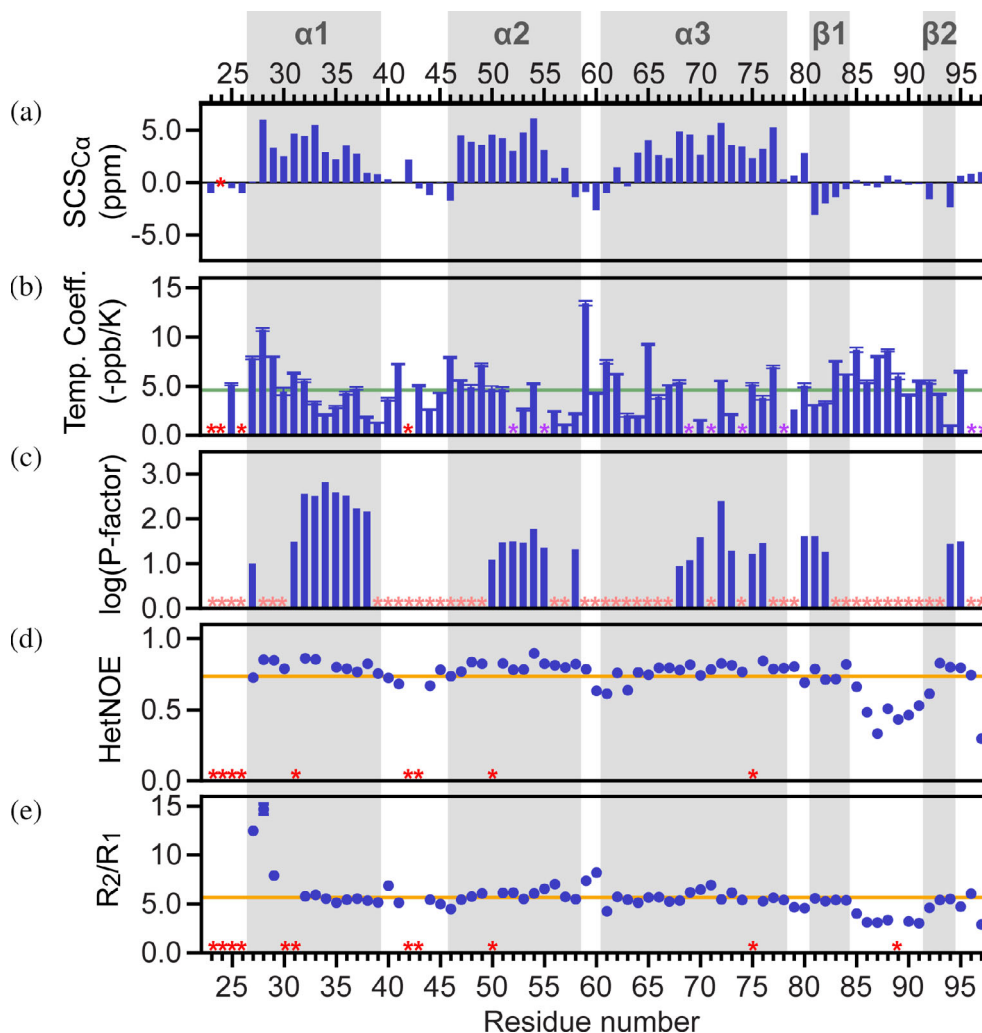
FIGURE 3 Secondary structure and dynamics of hH1.0$_{GD}$. (a) C$^\alpha$-derived secondary chemical shifts of hH1.0$_{GD}$. (b) Amide temperature coefficients derived from amide chemical shift changes as a function of temperature from 278 to 323 K. Values below the green line at −4.6 ppb/K are generally considered to be indicative of hydrogen bonds.[42] Purple stars highlight residues with nonlinear behavior. (c) Amide H/D exchange protection factors. Light red stars indicate residues that exchange faster than the experiment dead time. (d) Heteronuclear NOE values of hH1.0$_{GD}$ at 600 MHz. The orange line represents the average (0.73). (e) Ratios of transverse (R_2) and longitudinal (R_1) ^{15}N-relaxation rates of hH1.0$_{GD}$ at 600 MHz. Error bars are derived from the fits and the orange line represents the average (5.7). Unless otherwise specified, data were acquired at an ionic strength of 165 mM, pH 7.4, 10°C. Gray shading highlight regions populating secondary structures, and in a, b, d, and e, red stars indicate missing data points

(Figure 5a,b) (data retrieved in 2021). These structures were solved in complex with nucleosomes (PDBs: 7k5x, 6la8, 6la9, 7dbp, 5nl0, 4qlc, 5wcu) or with a protein partner (PDBs: 6n88, 6n89), except for a single X-ray structure of the *G. gallus* H5-GD in its unbound state (PDB id 1hst). Complex formation with DNA or the protein partner importin β (Impβ) occurs through an extended binding region, with the GD almost buried within the partners (Figure 5c,d). In both cases, α2 and α3 have many contacts to the partners, whereas α1 is mainly solvent-exposed (Figure 5a,c,d). Superposition of the unbound hH1.0$_{GD}$ structure (PDB: 6hq1) with these 10 structures revealed RMSDs of the C$^\alpha$-atoms between

1.5 and 2.2 Å (Figure 5b). This result suggests that the structure is highly conserved across species, as expected from the high sequence conservation (Figure 1c). Further, with the present structure of the unbound hH1.0$_{GD}$, it is now evident that complex formation with various partners occurs without geometrical adaptation of most of the backbone. Nonetheless, the unbound and bound structures differ in one particular site: L4 of the β-hairpin. Here, all the bound GDs (except PDB: 7db0, resolution 4.5 Å) are in the "closed" state, while the *G. gallus* unbound H5-GD crystal structure show both closed and open states, and the unbound hH1.0$_{GD}$ NMR structure in solution presented here, only the open state (Figure 5e).

TABLE 1 NMR and refinement statistics for hH1-GD structures

	hH1-GD$_{24-97}$
NMR distance and dihedral constraints	
Distance constraints	
Total NOE	702 (845)
Intraresidue	183
Interresidue	519
Sequential ($|i - j| = 1$)	191
Medium range ($|i - j| < 4$)	158
Long range ($|i - j| > 5$)	170
Intermolecular	—
Hydrogen bond restraints	0
Dihedral angle restraints (φ/ψ)	70/70
Structure statistics	
Violations (mean and SD)	
Distance constraints (Å)	0.030 ± 0.002
Dihedral angle constraints (°)	0.68 ± 0.05
Max. Dihedral angle violation (°)	4.66
Max. Distance constraint violation (Å)	0.315
Deviations from idealized geometry	
Bond lengths (Å)	0.006 ± 0.000
Bond angles (°)	0.781 ± 0.008
Impropers (°)	0.44 ± 0.01
Average pairwise r.m.s. deviation[a] (Å)	
Heavy	0.81 ± 0.04[b]
Backbone	0.41 ± 0.09[b]
Ramachandran plot statistics (%)	
Residues in most favored regions	93.2%
Residues in additionally allowed regions	6.8%
Residues in generously allowed regions	0%
Residues in disallowed regions	0%

[a]Pairwise r.m.s. deviation was calculated among 20 refined structures.
[b]Residues 28–95.

2.4 | Effect of positive charges on structure and stability of histone GDs

As highlighted above, the primary, secondary, and tertiary structures of H1-GD are highly conserved, both across species and isoforms (Figures 1b,c and 5b). The main difference in primary structure pertains to the occurrence and position of residues with charged side chains, suggesting these to be less important for the structure, but potentially relevant for stability and/or function. The charged side chains are well distributed in the primary and the tertiary structure of hH1.0$_{GD}$ (Figure 6a), with a net charge of −1 in α1, +3 in α2, +1 in α3, and positive charges in all loop regions. From pH titrations of the hH1.0$_{GD}$ followed by ^{15}N-^{1}H-HSQC spectra over the pH range 5.1–10.7, we found that the two histidines, His25 and His57, have pK$_a$ values of 6.3 ± 0.3 and 7.5 ± 0.2 (Figure S2), suggesting at least His57 to contribute to the overall positive charge of hH1.0$_{GD}$ at physiological pH (pH 7.0–7.4).

To investigate the influence of the charged side chains on the structure and stability of unbound hH1.0$_{GD}$, we designed, expressed and purified 11 charge variants of hH1.0$_{GD}$ (Figure 6b). In these variants, we changed the net charge from the WT value of +9 (disregarding the partial charge from especially His57), to a value between +5 and +13. This was done by combinations of (a) replacing different Lys with Gln, (b) substituting different uncharged, solvent exposed residues with Lys, and (c) replacing different Asp or Glu with Gln (Figure 6b). Additionally, we produced a variant with His57 replaced by Lys.

Using far-UV CD spectroscopy, the secondary structure content of the variants was evaluated. Except for the most charged variant (12K1-DE; +13), which had less helical structure at 283 K compared to the others due to destabilization (see below), no substantial differences in the helical content of the different variants compared to WT was observed, suggesting that the structure remained
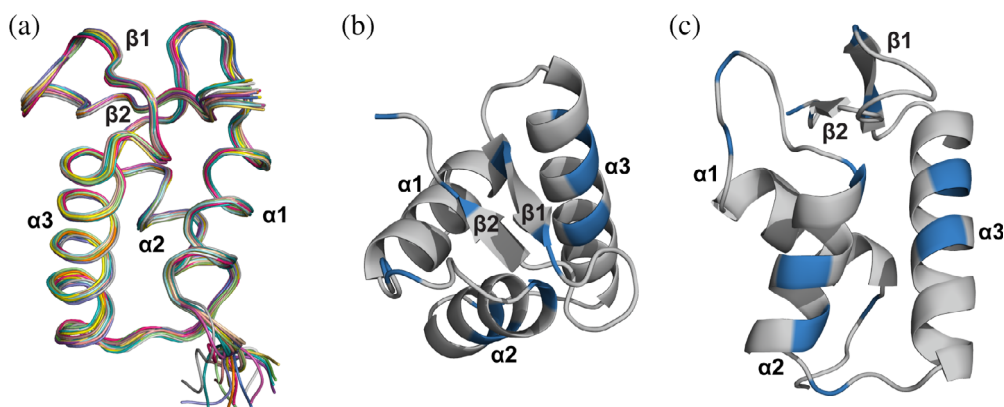

FIGURE 4 Solution structure of hH1.0$_{GD}$. (a) Ribbon structure of the 20 lowest energy structures of hH1.0$_{GD}$, having a backbone RMSD of 0.41 Å. (b,c) Lowest energy-structure of hH1.0$_{GD}$ from two different angles, with Lys and Arg highlighted in blue

intact in all cases (Figure S3). The thermal stability of all variants was subsequently quantified by following the change in ellipticity at 222 nm over a temperature range of 273–353 K (Figure S4), assuring reversibility of all variants. The resulting T_m values differed by up to 26 K, with 302 K for the least stable variant (12K1-DE) to 328 K for the most stable (6K1) (Figure 6b). Plotting the T_m values of the variants and WT versus their net charge revealed a trend of higher net positive charge resulting in lower thermal stability and vice versa (Figure 6c). This suggests that the abundance of positively charged side chains on the surface comes at the cost of stability. For all variants,
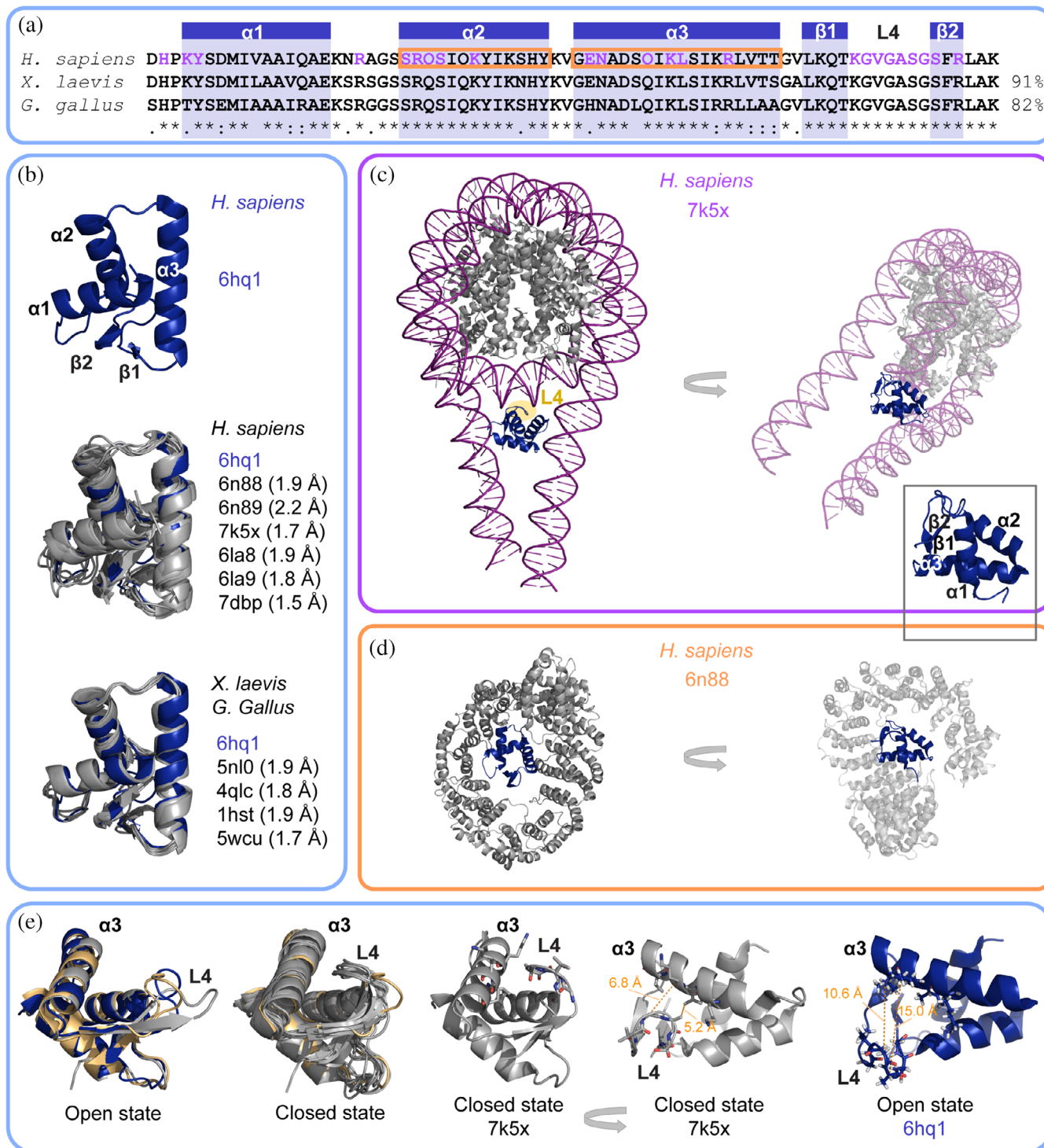

FIGURE 5 Legend on next page.

excluding 12K1-DE, standard Gibbs free energies for folding of the variants relative to WT, $\Delta\Delta G_{\text{N-D apparent (WT-MUT)}}$, were estimated at 293 K based on the average change in enthalpy, $\Delta H_{\text{average}}^{T_m}$ (Table S1; see Methods). The estimated $\Delta\Delta G_{\text{N-D apparent}}$ reflect the measured T_m values (Figure S6, Table S1) and suggest that removal of 2–4 positive charges from the WT gives a stability reward in the range of -1 to -3 kJ/mol, while addition of just 2 charges gives a penalty of 3–4 kJ/mol. To further substantiate the effect of electrostatic repulsion on GD stability, we measured the T_m of WT $hH1.0_{\text{GD}}$ at different ionic strengths (I_s) (Figure S5). Increasing I_s enhanced the thermal stability of $hH1.0_{\text{GD}}$ with T_m increasing from 310 K at 1 mM to 325 K at 300 mM. The thermal stability of $hH1.0_{\text{GD}}$ versus the square root of I_s is linear (Figure 6d), consistent with the Debye-Hückel-type behavior reported previously for proteins with net destabilizing electrostatic interactions.[44] These observations are also consistent with the net electrostatic interactions on the GD surface being repulsive. The change relative to $I_{s,165 \text{ mM}}$ in standard Gibbs free energies for folding of the WT changed from 5.8 ± 0.2 kJ/mol to -2.1 ± 0.1 kJ/mol between 1 mM and 300 mM ionic strength (Figure S7). Thus, in conclusion, changing the net charge of $hH1.0_{\text{GD}}$ does not have a detectable effect on its structure, but it does affect the thermal stability considerably.

3 | DISCUSSION

Until now, the structure of the unbound GD of human H1.0 has not been known, which has limited the mechanistic understanding of the structural adaptation of the GD upon engaging with nucleosomes. With the present structure of unbound $hH1.0_{\text{GD}}$, it is apparent that the overall structure is unperturbed by complex formation with nucleosomes, except for the β-hairpin. The two different conformations of the β-hairpin present in the crystal structure of the unbound GD from avian H5 (1hst)[33] were defined as either an "open" or a "closed" state with respect to α3. In silico studies have suggested that the closed state is the dominant conformation of unbound GD in solution,[34,35] but here we detected only the open state. The closed state, on the other hand, is found in the structures of GDs in complex with nucleosomes (Figure 5) (except PDB: 7dbp), where L4 is in contact with DNA and maximize contacts with the DNA backbone rather than the grooves. The closed conformation is also found in the low-resolution structures of the complex with the protein partner Impβ (PDBs: 6n88, 6n89). As only a single Lys is present at the N-terminal of the seven residues long L4 (Figure 5a), we do not expect the sampling of the open and closed states to be influenced substantially by changing surface electrostatics. In summary, our data suggest that upon complex formation, the β-hairpin is the only part of the GD undergoing substantial changes in backbone conformation, moving from a flexible, open conformation to a restricted, closed conformation.

The structure of the GDs is highly conserved across species and isoforms, with the most pronounced differences in primary structure being the amount and positions of residues with charged side chains. In the present work, we show that the addition or removal of positive side chains in $hH1.0_{\text{GD}}$ do not alter the structure but affect the conformational stability. Using 11 charge variants with net charges between $+5$ and $+13$, we found that decreasing the positive net charge increased stability and vice versa. The dependence on I_s further supports the conclusion that the relatively low stability of the $hH1.0_{\text{GD}}$ WT is caused by destabilization by charge repulsion, which was also found in studies of the yeast linker

FIGURE 5 Comparison of GD structures from species with >80% sequence identity to $hH1.0_{\text{GD}}$ and their complexes. (a) Alignment of GD sequences (residues 24–97 of the human H1) from human, *X. laevis* and *G. gallus* by Clustal Omega, with sequence identity to $hH1.0_{\text{GD}}$ shown to the right. The secondary structure elements of human $hH1.0_{\text{GD}}$ (PDB: 6hq1) are highlighted with blue boxes, orange boxes highlight the region close to Impβ in the human H1.0-Imp7:Impβ complex (PDBs: 6n88, 6n89),[43] and residues in contact with DNA in a GD–chromatosome complex (PDB: 7k5x) are highlighted in purple.[18] (b) Unbound $hH1.0_{\text{GD}}$ structure (PDB: 6hq1, blue) (top), superimposed with complexed human GD structures (middle, gray) and unbound and complexed GD structures with sequence identity to $hH1.0_{\text{GD}} > 80\%$ (*X. laevis*- or *G. gallus* GD) (bottom, gray). The C^α RMSD to PDB: 6hq1 (residues 26–94 in human) of each structure is shown in parenthesis. (c) Complex between human H1.0 and a chromatosome at 2.9 Å (PDB: 7k5x[18]), at two different angles, and with the GD structure highlighted in the right panel. L4 is highlighted with yellow shading. (d) Human H1-Imp7:Impβ complex at 6.2 Å (PDB: 6n88,[43] Imp7 not shown for clarity), at two different angles, and with the GD structure highlighted in the right panel. The orientation of the GD in the right panels of (c) and (d) is identical to the $hH1.0_{\text{GD}}$ structures in the gray box insert. (e) The "open" and "closed" states of the L4 of the β-hairpin. From the left: 1) overlay of all the GD structures in open state (PDB: 6hq1; blue, PDB: 1hstA; grey, PDB: 7dbp; orange). 2) overlay of all the bound GD structures (PDBs: 6n88, 6n89, 7k5x, 6la8, 6la9, 7dbp, 5 nl0, 4qlc, 5wcu) and PDB: 1hstB, which are all in the closed state except PDB: 7dbp (highlighted in orange). 3 + 4) PDB: 7k5x from two angles as example of the closed state, with side chains of L4 and α3 in proximity in the closed state shown as sticks and distances between selected residues in orange. 5) PDB: 6hq1 from the same angle as in 4), highlighting the larger distance between corresponding selected residues of α3 and L4 in the open state

FIGURE 6 Effect of charges on hH1.0$_{GD}$ stability. (a) Overview of the position of residues with charged side chains in the primary and tertiary structure of hH1.0$_{GD}$. (b) Overview of variants, their substitutions, net charge and the measured T_ms. (c) T_m plotted against net charge of the variants. (d) Thermal stability of WT hH1.0$_{GD}$ as a function of the square root of the ionic strength

(a)
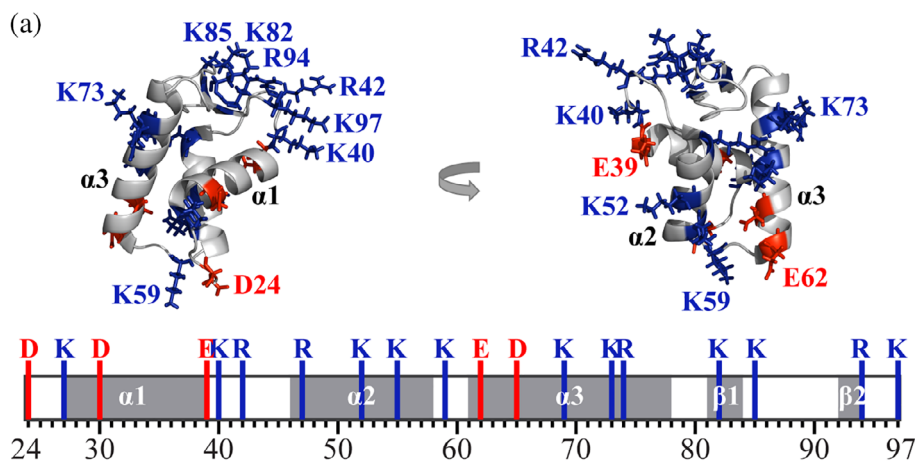
(b)

Variant	Substitutions	Net charge	T_m (K)
WT		+9	321.8 ± 0.1
6K1	K82Q, K52Q, K85Q, K73Q	+5	327.8 ± 0.1
6K2	K85Q, K73Q, K40Q, K97Q	+5	325.7 ± 0.1
8K1	K82Q, K52Q	+7	323.3 ± 0.1
8K2	K85Q, K73Q	+7	326.4 ± 0.1
8K3	K59Q, K69Q	+7	325.9 ± 0.1
H57K	H57K	+10	315.6 ± 0.1
2E2Q	E39Q, E62Q	+11	313.3 ± 0.1
12K1	A34K, Q67K	+11	313.4 ± 0.1
12K2	L70K, S90K	+11	316.5 ± 0.1
2E2K	E39K, E62K	+13	313.1 ± 0.1
12K1-DE	A34K, Q67K, D30N, E39Q	+13	301.6 ± 0.3

(c)

(d) $R^2 = 0.94$
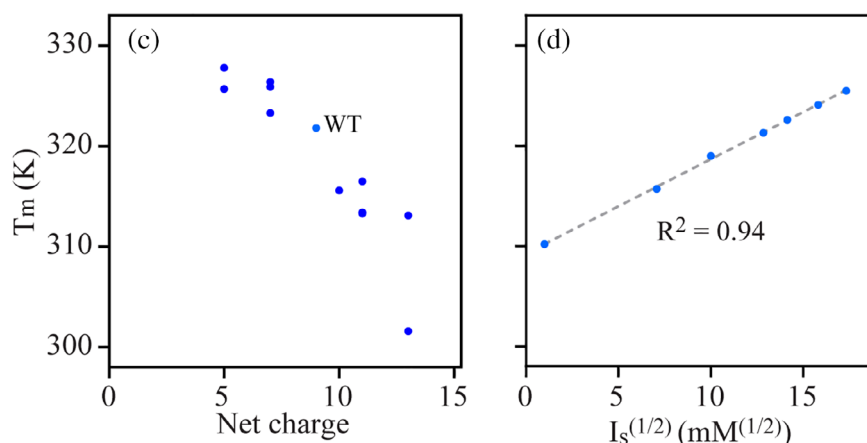
histone Hho1p.[45] Hence, our data indicate that the conservation of the Lys and Arg of GDs across species and isoforms is likely of functional importance, rather than important for structure. The high positive net charge of hH1.0$_{GD}$ comes at the cost of stability, and the winged helix-turn-helix fold is pushed to the limit of the amount of charge it can carry. Additional positive charge required for the high-affinity interaction with DNA is likely

achieved through the highly positively charged disordered tails. Our CD spectroscopy data suggested that at body temperature (37°C), ~8% of the H1 population will have GD in an unfolded state (Figure 2b), and removing two positive charges lowers the population of the unfolded state to 2%–5% depending on the position. However, even substantial changes in the folding stability will make no significant change in the effective concentration

of the folded state and thus of the conformation that binds DNA.[46] Therefore, compared to the loss of charges, the unfolded state likely plays a minor role in binding.

Besides having conserved positions to confer a certain binding site geometry, the charged side chains may also encode a specific degree of stability. Considering the electrostatic nature of the GD–DNA interaction and the destabilizing effect on the structure of the high charge density, screening of the charges by binding to the highly negatively charged DNA will likely add to the stabilization of the complex. The stability of the hH1.0$_{GD}$ changed by 8 kJ/mol from 0 to 300 mM I_s just as the stability of the GDII of yeast linker histone Hho1p increases in the presence of tetrahedral anions.[47] This screening effect may be modulated by posttranslational modifications. Although the functional relevance of posttranslational modifications of H1.0 remains to be fully uncovered, it includes regulation of chromatin condensation and transcriptional regulation through altered interaction networks or/and increasing the dynamic exchange of H1 on chromatin.[48–50] Lysine acetylation is most common in the H1 C-tail, but acetylation and phosphorylation are also found in the GD, including, for example, lysine acetylation of K85 and phosphorylation of S66 and T84.[48,49,51] Such modifications, whose patterns depend on the cell type, may weaken the interaction with DNA by removing electrostatic repulsion in the unbound GD structure, and hence decrease the stability of the complex.

4 | MATERIALS AND METHODS

4.1 | Expression and purification of hH1.0$_{GD}$ and variants

GST-fused hH1.0$_{GD}$ was expressed and purified as previously described.[40] For a small ubiquitin-like modifier (SUMO) purification construct, DNA coding for the sequence corresponding to residues D24–K97 from human H1.0 was inserted into a modified pET24b vector, which also codes for a hexahistidine SUMO-tag added to the N-terminal of the proteins. Mutants were made using the QuickChange kit from Agilent using primers purchased form TAG Copenhagen. Expression in *Escherichia coli* BL21-(DE3) (Biolabs) cells of the SUMO-tagged hH1.0$_{GD}$ WT and variants were done in either Sigma Aldrich high salt LB-broth medium, or M9 minimal medium containing ^{15}N-NH$_4$Cl, or M9 minimal medium containing ^{15}N-NH$_4$Cl and $^{13}C_6$-glucose. Expression was induced at OD$_{600}$ 0.5–0.8 with 0.1 mM IPTG and the cells were grown for 4 hr at 37°C under shaking at 180 rpm. Cells were harvested by centrifugation at 5,000g for 20 min and resuspended in Buffer A (50 mM Tris pH 8.0,

20 mM imidazole, 200 mM NaCl, 10% [v/v] glycerol) and lysed through a cell disrupter (Constant Systems Ltd.). The lysate was centrifuged at 20,000g for 45 min and the supernatant passed over 5 ml Ni-NTA resin (Qiagen) preequilibrated in buffer A and subsequently washed with 50 ml Buffer B (50 mM Tris pH 8.0, 10 mM imidazole, 1 M NaCl, 10% [v/v] glycerol) and 50 ml Buffer A. The proteins were eluted with Buffer A added 500 mM imidazole and diluted to 100 mM imidazole with Buffer A before adding 1 mM DTT and 0.1 mg His-tagged ULP1-protease, purified as described in the literature[52] to cleave off the tag leaving no cloning artifacts. After cleavage, the mixtures were diluted 1:1 (v/v) with Buffer A before passing it over the 5 ml of Ni-NTA resin to remove uncleaved product. The collected flow-through was dialyzed overnight against 50 mM Na$_2$HPO$_4$ pH 9 and was purified on a HiTrap SP FF 5 ml column (Sigma Aldrich) to remove DNA using a ÄKTA pure 25 chromatography system (GE Healthcare). A gradient from 0% to 70% 50 mM Na$_2$HPO$_4$ pH 9, 1 M NaCl over 25 column volumes was used. The fractions containing pure hH1.0$_{GD}$ or variants were pooled and dialyzed into 1x TBS buffer (10 mM Tris, 157 mM KCl, 0.1 mM EDTA, pH 7.4, I_s = 165 mM), subsequently flash frozen with liquid nitrogen and stored at −20°C.

4.2 | Circular dichroism

Far-UV CD spectra were recorded using a Jasco-J-815 installed with a Peltier controlled cuvette holder. All spectra were recorded at 10°C between 260 and 195 nm, data pitch was 0.5 nm and a digital integration time of 2 s, path length of 0.1 cm and a scan speed of 50 nm/s, accumulating 10 scans. Only measurements at an HT below 700 V were included, and identical setting was used to record a spectrum of the buffer, which was then subtracted. The proteins were dissolved in TBS buffer, pH 7 at RT at a concentration of 20 ± 0.5 μM. The ellipticity was converted to mean residue weight ellipticity using Equation (1).

$$[\theta]_{MRW} = \frac{\frac{MW}{(n-1)} m\deg}{10\,c\,d} \tag{1}$$

where $[\theta]_{MRW}$ is the mean residue weight ellipticity, c is the concentration in g/L, n is the number of residues, d is the path length in cm, and MW is the molecular weight in Da.

To determine the thermal stability, melting experiments were performed from 283 to 353 K in increments of 1 K/min and monitoring the ellipticity change at 222 nm. Ellipticity was sampled every 0.1°C, and the

sample was allowed to return to the start temperature after which a spectrum was recorded for assessing reversibility. The thermal melting curves were fitted to the following equation:

$$y = \frac{(m_N T + y_N) + (m_D T + y_D)\exp\left(-\frac{\Delta H\left(1 - \frac{T}{T_m}\right)}{RT}\right)}{1 + \exp\left(-\frac{\Delta H\left(1 - \frac{T}{T_m}\right)}{RT}\right)}$$

where y is the observed signal, y_N and y_D are the baseline intercepts before and after transition, respectively, m_N and m_D are the slopes of the baselines before and after transition, respectively, ΔH is the van't Hoff enthalpy at T_m, T is the temperature, T_m is the melting temperature, and R is the gas constant. For calculation of the change in stability $\Delta\Delta G_{\text{N-Dapparent(WT-MUT)}}$, we made the assumptions that ΔC_p is temperature independent and that the changes in ΔC_p are close to zero. We used the following equation (based on the literature[53]) to calculate $\Delta\Delta G_{\text{N-D}}$ apparentK at 298K:

$$\Delta\Delta G_{N-D\,\text{apparent}}(T) \approx \frac{-\Delta H_{\text{average}}^{Tm} T}{\left(T_m^{WT} T_m^{Mut}\right)} \Delta T_m$$

where T is the temperature, $\Delta H_{\text{average}}^{Tm}$ is the average folding enthalpy at T_m of the included protein variants, T_m^{WT} and T_m^{Mut} are the melting temperatures of WT and protein variant, respectively, and ΔT_m is the difference in melting temperature between the WT and the protein variant ($\Delta T_m = T_m^{mut} - T_m^{WT}$).

4.3 | NMR spectroscopy

Unless otherwise specified, all NMR samples contained 100–200 μM ^{15}N-hH1.0$_{GD}$ or 925 μM ^{13}C,^{15}N-hH1.0$_{GD}$ in TBS buffer (with an ionic strength of 165 mM adjusted with KCl), pH 7.4 (at 283 K), 10% D$_2$O (v/v), and 0.7 mM 4,4-dimethyl-4-silapentane-1-sulfonic acid (DSS). Unless otherwise specified, all NMR spectra were acquired at 283 K on Bruker AVANCE III 600-, 750-MHz (^{1}H) spectrometers equipped with cryogenic probes or a Varian 800 MHz (^{1}H) equipped with a room temperature probe. Free induction decays were transformed and visualized in NMRPipe[54] or Topspin (Bruker Biospin) and analyzed using the CcpNmr Analysis software.[55] Proton chemical shifts were referenced internally to DSS at 0.00 ppm, with heteronuclei referenced by relative gyromagnetic ratios.

Assignments of backbone nuclei of hH1.0$_{GD}$ were performed manually from the analysis of ^{15}N-^{1}H-HSQC, HNCACB, HNCOCACB, HNCOCA, HNCO, HCCH-

TOCSY, and ^{15}N-^{1}H-TOCSY-HSQC spectra acquired with nonuniform sampling[56] using standard pulse sequences. SCSs of hH1.0$_{GD}$ were calculated based on C$^\alpha$ shifts and published random coil values.[41] NOEs were picked from aliphatic and aromatic ^{13}C-NOESY-HSQC and ^{15}N-NOESY-HSQC spectra recorded with mixing times of 130, 130, and 130 ms, respectively.

Amide temperature coefficients were calculated by fitting H^N chemical shifts from a series of ^{15}N-^{1}H-HSQC spectra of ^{15}N-hH1.0$_{GD}$ at 278–323 K (steps of 5 K) versus temperature to a linear model using the CcpNmr Analysis software.[55]

To determine the pKa values of the histidines and their surrounding residues, ^{15}N-^{1}H-HSQC spectra were recorded of a pH titration with 130 μM ^{15}N-hH1.0$_{GD}$ in TBS buffer at pH 5.1, 6.1, 6.4, 6.6, 7.2, and 10.7. To calculate the pKa values, the chemical shift differences from shifting residues at each pH compared to their shift at pH 5.1 were extracted and the data was normalized so that all data points lie between 0 at lowest pH (no protonation) and 1 at highest pH (full protonation) using the following equation:

$$\text{Normalized chemical shifts} = \frac{\text{Chemical shift at given pH}}{\text{Chemical shifts at highest pH}}$$

The normalized chemical shifts were plotted against the pH values and fitted with a modified Henderson–Hasselbalch equation[57] in GraphPad Prism to determine the pKa.

For hydrogen-to-deuterium exchange experiments, the sample was dialyzed in TBS buffer and the pH adjusted to 7.4 at 278 K before freeze-drying. For NMR analysis, the freeze-dried sample was dissolved in 350 μl 100% (v/v) D$_2$O and loaded immediately into a precooled NMR tube and the first HSQC was recorded at 278 K, 3 min after adding the sample to the tube. ^{15}N-^{1}H HSQC spectra were recorded for 3 min each and a total of 50 time points recorded, finalizing recording after ~2.5 h. From the assigned ^{15}N-^{1}H-HSQC spectrum of hH1.0$_{GD}$, peak heights were extracted, and the experimental rate constants determined using CcpNMR analysis. Intrinsic exchange rates were calculated using SPHERE https://protocol.fccc.edu/research/labs/roder/sphere/.[58]

T_1- and T_2 ^{15}N-relaxation times of ^{15}N-hH1.0$_{GD}$ were determined from two series of ^{15}N-^{1}H-HSQC spectra with varying relaxation delays recorded at 600 MHz (^{1}H), using 12 (20–1,200 ms) and 12 (16–256 ms) different relaxation delays for T_1 and T_2, respectively, including triplicate measurements. T_1- and T_2 relaxation experiments were recorded with a recycle delay of 2.5 s. The relaxation decays were fitted to single exponentials and relaxation times determined using CcpNmr Analysis

software.[55] HetNOEs were measured on ^{15}N-hH1.0$_{GD}$ at 600 MHz with saturation of ^{1}H for 5 s and analyzed using CcpNmr Analysis software.[55]

4.4 | Structure calculations

The backbone chemical shifts of hH1.0$_{GD}$ were submitted to TALOS+[59] to extract dihedral angle restraints. NOE peaks were picked manually in the ^{1}H, ^{15}N-NOESY-HSQC-, aliphatic- and aromatic ^{1}H, ^{13}C-NOESY-HSQC spectra, and the peak list used for semi-automated NOE assignment and structure calculation with CYANA (version 3.97).[60] Iteratively, the structures and assignments were checked manually, modified if needed, and structures recalculated. The structures were further refined with Xplor-NIH (version 2.44)[61] using standard protocols and the NOE- and TALOS restraints, and 200 structures were calculated. The hH1.0$_{GD}$ structure was further refined with the implicit water solvation potential EEFx (Effective Energy Function for Xplor-NIH).[62] The 20 lowest energy structures without distance- and dihedral angle violations above 0.5 Å and 5°, respectively, were selected to represent the structure of hH1.0$_{GD}$. The quality of the structures was evaluated with PROCHECK-NMR, and structures were visualized in PyMOL (Schrödinger).

4.5 | Data deposition

The chemical shifts of WT hH1.0$_{GD}$ have been deposited in the NMR BioMagResBank accession number 34318 and the three-dimensional structure in the protein data bank under the PDB accession code 6hq1.

AUTHOR CONTRIBUTIONS
Jacob H. Martinsen: Conceptualization (supporting); data curation (supporting); formal analysis (lead); investigation (lead); validation (lead); writing – review and editing (lead). **Daniel Saar:** Formal analysis (supporting); investigation (supporting); writing – review and editing (supporting). **Catarina B. Fernandes:** Formal analysis (supporting); investigation (supporting); writing – review and editing (supporting). **Benjamin Schuler:** Conceptualization (supporting); formal analysis (supporting); funding acquisition (supporting); writing – review and editing (supporting). **Katrine Bugge:** Concepturalization (lead); data curation (lead); formal analyses (lead); investigation (lead); validation (lead); writing – review and editing (lead). **Birthe B. Kragelund:** Conceptualization (lead); formal analysis (supporting); investigation (supporting); writing – review and editing (lead); funding acquisition (lead).

ORCID
Jacob H. Martinsen https://orcid.org/0000-0001-9874-1138
Daniel Saar https://orcid.org/0000-0001-5197-4591
Catarina B. Fernandes https://orcid.org/0000-0002-6198-3173
Benjamin Schuler https://orcid.org/0000-0002-5970-4251
Katrine Bugge https://orcid.org/0000-0002-6286-6243
Birthe B. Kragelund https://orcid.org/0000-0002-7454-1761

REFERENCES
1. Millard PS, Bugge K, Marabini R, Boomsma W, Burow M, Kragelund BB. IDDomainSpotter: Compositional bias reveals domains in long disordered protein regions—Insights from transcription factors. Protein Sci. 2020;29:169–183.
2. Luger K, Mäder AW, Richmond RK, Sargent DF, Richmond TJ. Crystal structure of the nucleosome core particle at 2.8 Å resolution. Nature, 1997;389:251–260. http://dx.doi.org/10.1038/38444
3. Fyodorov DV, Zhou B, Skoultchi AI, Bai Y. Emerging roles of linker histones in regulating chromatin structure and function. Nat Rev Mol Cell Biol. 2018;19:192–206.
4. van Emmerik CL, van Ingen H. Unspinning chromatin: Revealing the dynamic nucleosome landscape by NMR. Prog Nucl Magn Reson Spectrosc. 2019;110:1–19.
5. Cutter AR, Hayes JJ. A brief review of nucleosome structure. FEBS Lett. 2015;589:2914–2922.
6. Panyim S, Chalkley R. High resolution acrylamide gel electrophoresis of histones. Arch Biochem Biophys. 1969;130:337–346.
7. Allan J, Hartman PG, Crane-Robinson C, Aviles FX. The structure of histone H1 and its location in chromatin. Nature. 1980; 288:675–679.
8. Hergeth SP, Schneider R. The H1 linker histones: Multifunctional proteins beyond the nucleosomal core particle. EMBO Rep. 2015;16:1439–1453.
9. Sandaltzopoulos R, Blank T, Becker PB. Transcriptional repression by nucleosomes but not H1 in reconstituted preblastoderm Drosophila chromatin. EMBO J. 1994;13:373–379.
10. Yusufova N, Kloetgen A, Teater M, et al. Histone H1 loss drives lymphoma by disrupting 3D chromatin architecture. Nature. 2021;589:299–305.

11. Talbert PB, Ahmad K, Almouzni G, et al. A unified phylogeny-based nomenclature for histone variants. Epigenet Chromatin. 2012;5:7.

12. Zlatanova J, Doenecke D. Historie H1°: a major player in cell differentiation?. The FASEB Journal, 1994;8:1260–1268. http://dx.doi.org/10.1096/fasebj.8.15.8001738

13. Hao F, Kale S, Dimitrov S, Hayes JJ. Unraveling linker histone interactions in nucleosomes. Curr Opin Struct Biol. 2021;71:87–93.

14. Zhou B-R, Feng H, Ghirlando R, Li S, Schwieters CD, Bai Y. A small number of residues can determine if linker histones are bound on or off dyad in the chromatosome. J Mol Biol. 2016;428:3948–3959.

15. Misteli T, Gunjan A, Hock R, Bustin M, Brown DT. Dynamic binding of histone H1 to chromatin in living cells. Nature. 2000;408:877–881.

16. Lever MA, Th'ng JPH, Sun X, Hendzel MJ. Rapid exchange of histone H1.1 on chromatin in living human cells. Nature. 2000;408:873–876.

17. Singer DS, Singer MF. Studies on the interaction of H1 histone with superhelical DNA: Characterization of the recognition and binding regions of H1 histone. Nucleic Acids Research, 1976;3:2531–2548. http://dx.doi.org/10.1093/nar/3.10.2531

18. Zhou B, Feng H, Kale S, et al. Distinct structures and dynamics of chromatosomes with different human linker histone isoforms. Mol Cell. 2021;81:166–182.

19. Heidarsson PO, Mercadante D, Sottini A, et al. Release of linker histone from the nucleosome driven by polyelectrolyte competition with a disordered protein. Nat Chem. 2022. http://dx.doi.org/10.1038/s41557-021-00839-3

20. Bednar J, Garcia-Saez I, Boopathi R, et al. Structure and Dynamics of a 197 bp Nucleosome in Complex with Linker Histone H1. Molecular Cell, 2017;66:729. http://dx.doi.org/10.1016/j.molcel.2017.05.018

21. Adhireksan Z, Sharma D, Lee PL, Davey CA. Near-atomic resolution structures of interdigitated nucleosome fibres. Nat Commun. 2020;11:1–13.

22. Zhou B-R, Jiang J, Feng H, Ghirlando R, Xiao TS, Bai Y. Structural mechanisms of nucleosome recognition by linker histones. Mol Cell. 2015;59:628–638.

23. Zhou B-R, Jiang J, Ghirlando R, et al. Revisit of reconstituted 30-nm nucleosome arrays reveals an ensemble of dynamic structures. J Mol Biol. 2018;430:3093–3110.

24. Wang S, Vogirala VK, Soman A, et al. Linker histone defines structure and self-association behaviour of the 177 bp human chromatosome. Sci Rep. 2021;11:380.

25. Zhou B-R, Feng H, Kato H, et al. Structural insights into the histone H1-nucleosome complex. Proc Natl Acad Sci U S A. 2013;110:19390–19395.

26. Song F, Chen P, Sun D, et al. Cryo-EM study of the chromatin fiber reveals a double helix twisted by tetranucleosomal units. Science. 2014;344:376–380.

27. Öztürk MA, Cojocaru V, Wade RC. Toward an ensemble view of chromatosome structure: A paradigm shift from one to many. Structure. 2018;26:1050–1057.

28. Liao LW, Cole RD. Condensation of dinucleosomes by individual subfractions of H1 histone. J Biol Chem. 1981;256:10124–10128.

29. Th'ng JPH, Sung R, Ye M, Hendzel MJ. H1 family histones in the nucleus. J Biol Chem. 2005;280:27809–27814.

30. Brown DT, Gunjan A, Alexander BT, Sittman DB. Differential effect of H1 variant overproduction on gene expression is due to differences in the central globular domain. Nucleic Acids Res. 1997;25:5003–5009.

31. Cerf C, Lippens G, Ramakrishnan V, et al. Homo- and heteronuclear two-dimensional NMR studies of the globular domain of histone H1: Full assignment, tertiary structure, and comparison with the globular domain of histone H5. Biochemistry. 1994;33:11079–11086.

32. Clore GM, Gronenborn AM, Nilges M, Sukumaran DK, Zarbock J. The polypeptide fold of the globular domain of histone H5 in solution. A study using nuclear magnetic resonance, distance geometry and restrained molecular dynamics. EMBO J. 1987;6:1833–1842.

33. Ramakrishnan V, Finch JT, Graziano V, Lee PL, Sweet RM. Crystal structure of globular domain of histone H5 and its implications for nucleosome binding. Nature. 1993;362:219–223.

34. Öztürk MA, Pachov GV, Wade RC, Cojocaru V. Conformational selection and dynamic adaptation upon linker histone binding to the nucleosome. Nucleic Acids Res. 2016;44:6599–6613.

35. Woods DC, Wereszczynski J. Elucidating the influence of linker histone variants on chromatosome dynamics and energetics. Nucleic Acids Res. 2020;48:3591–3604.

36. Wu H, Dalal Y, Papoian GA. Binding dynamics of disordered linker histone H1 with a nucleosomal particle. J Mol Biol. 2021;433:166881.

37. Bugge K, Brakti I, Fernandes CB, et al. Interactions by disorder – A matter of context. Front Mol Biosci. 2020;7:110.

38. Staby L, Due AD, Ben Achim Kunze M, Louise Mønster Jørgensen M, Skriver K, Kragelund BB. Flanking disorder of the folded αα-hub domain from radical induced cell death1 affects transcription factor binding by ensemble redistribution. J Mol Biol. 2021;433:167320.

39. Staby L, Kemplen KR, Stein A, et al. Disorder in a two-domain neuronal Ca2+−binding protein regulates domain stability and dynamics using ligand mimicry. Cell Mol Life Sci. 2021;78:2263–2278.

40. Borgia A, Borgia MB, Bugge K, et al. Extreme disorder in an ultrahigh-affinity protein complex. Nature. 2018;555:61–66.

41. Kjaergaard M, Brander S, Poulsen FM. Random coil chemical shift for intrinsically disordered proteins: Effects of temperature and pH. J Biomol NMR. 2011;49:139–149.

42. Cierpicki T, Otlewski J. Amide proton temperature coefficients as hydrogen bond indicators in proteins. J Biomol NMR. 2001;21:249–261.

43. Ivic N, Potocnjak M, Solis-Mezarino V, Herzog F, Bilokapic S, Halic M. Fuzzy interactions form and shape the histone transport complex. Mol Cell. 2019;73:1191–1203.

44. de los Rios MA, Plaxco KW. Apparent Debye−Huckel Electrostatic Effects in the Folding of a Simple, Single Domain Protein. Biochemistry, 2005;44:1243–1250. http://dx.doi.org/10.1021/bi048444l

45. Sanderson A, Stott K, Stevens TJ, Thomas JO. Engineering the structural stability and functional properties of the GI domain

into the intrinsically unfolded GII domain of the yeast linker histone Hho1p. J Mol Biol. 2005;349:608–620.

46. Teilum K, Olsen JG, Kragelund BB. Protein stability, flexibility and function. Biochim Biophys Acta Proteins Proteomics. 2011; 1814:969–976.

47. Ali T, Thomas JO. Distinct properties of the two putative "globular domains" of the yeast linker histone, Hho1p. J Mol Biol. 2004;337:1123–1135.

48. Izzo A, Schneider R. The role of linker histone H1 modifications in the regulation of gene expression and chromatin dynamics. Biochim Biophys Acta Gene Regul Mech. 2016;1859: 486–495.

49. Li Y, Li Z, Dong L, et al. Histone H1 acetylation at lysine 85 regulates chromatin condensation and genome stability upon DNA damage. Nucleic Acids Res. 2018;46:7716–7730.

50. Kamieniarz K, Izzo A, Dundr M, et al. A dual role of linker histone H1.4 Lys 34 acetylation in transcriptional activation. Genes Dev. 2012;26:797–802.

51. Starkova TY, Artamonova TO, Ermakova VV, Chikhirzhina EV, Khodorkovskii MA, Tomilin AN. The profile of post-translational modifications of histone H1 in chromatin of mouse embryonic stem cells. Acta Naturae. 2019;11: 82–91.

52. Reverter D, Lima CD. Preparation of SUMO proteases and kinetic analysis using endogenous substrates. Methods Mol Biol. 2009;497:225–239.

53. Pucci F, Bourgeas R, Rooman M. Predicting protein thermal stability changes upon point mutations using statistical potentials: Introducing HoTMuSiC. Sci Rep. 2016;6:23257.

54. Delaglio F, Grzesiek S, Vuister GW, Zhu G, Pfeifer J, Bax A. NMRPipe: A multidimensional spectral processing system based on UNIX pipes. J Biomol NMR. 1995;6:277–293.

55. Vranken WF, Boucher W, Stevens TJ, et al. The CCPN data model for NMR spectroscopy: Development of a software pipeline. Proteins Struct Funct Bioinforma. 2005;59:687–696.

56. Orekhov VY, Jaravine VA. Analysis of non-uniformly sampled spectra with multi-dimensional decomposition. Prog Nucl Magn Reson Spectrosc. 2011;59:271–292.

57. Chan C-H, Wilbanks CC, Makhatadze GI, Wong K-B. Electrostatic contribution of surface charge residues to the stability of a thermophilic protein: Benchmarking experimental and predicted pKa values. PLoS One. 2012;7:e30296.

58. Zhang Y-Z Protein and peptide structure and interactions studied by hydrogen exchange and NMR [PhD thesis]; 1998.

59. Shen Y, Delaglio F, Cornilescu G, Bax A. TALOS+: A hybrid method for predicting protein backbone torsion angles from NMR chemical shifts. J Biomol NMR. 2009;44:213–223.

60. Güntert P. Automated NMR protein structure calculation. Prog Nucl Magn Reson Spectrosc. 2003;43:105–125.

61. Schwieters CD, Kuszewski JJ, Tjandra N, Clore GM. The Xplor-NIH NMR molecular structure determination package. J Magn Reson. 2003;160:65–73.

62. Tian Y, Schwieters CD, Opella SJ, Marassi FM. A practical implicit solvent potential for NMR structure calculation. J Magn Reson. 2014;243:54–64.

SUPPORTING INFORMATION

Additional supporting information may be found in the online version of the article at the publisher's website.